*sustainability*

MDPI

*Article*

# Interdecadal Variations in Agricultural Drought Monitoring Using Land Surface Temperature and Vegetation Indices: A Case of the Amahlathi Local Municipality in South Africa

**Phumelelani Mbuqwa [1,2], Hezekiel Bheki Magagula [1], Ahmed Mukalazi Kalumba [1,2] and Gbenga Abayomi Afuye [1,2,*]**

[1] Department of Geography and Environmental Science, University of Fort Hare, Private Bag X1314, Alice 5700, Eastern Cape Province, South Africa; mbuqwap@gmail.com (P.M.); hmagagula@ufh.ac.za (H.B.M.); akalumba@ufh.ac.za (A.M.K.)

[2] Geospatial Application, Climate Change and Environmental Sustainability Lab–GACCES, University of Fort Hare, Alice 5700, Eastern Cape Province, South Africa

* Correspondence: afuyeabayomi@gmail.com

**Abstract:** Agricultural droughts in South Africa, particularly in the Amahlathi Local Municipality (ALM), significantly impact socioeconomic activities, sustainable livelihoods, and ecosystem services, necessitating urgent attention to improved resilience and food security. The study assessed the interdecadal drought severity and duration in Amahlathi's agricultural potential zone from 1989 to 2019 using various vegetation indicators. Landsat time series data were used to analyse the land surface temperature (LST), soil-adjusted vegetation index (SAVI), normalized difference vegetation index (NDVI), and standardized precipitation index (SPI). The study utilised GIS-based weighted overlay, multiple linear regression models, and Pearson's correlation analysis to assess the correlations between LST, NDVI, SAVI, and SPI in response to the agricultural drought extent. The results reveal a consistent negative correlation between LST and NDVI in the ALM, with an increase in vegetation ($R^2$ = 0.9889) and surface temperature. LST accuracy in dry areas increased to 55.8% in 2019, despite dense vegetation and a high average temperature of 40.12 °C, impacting water availability, agricultural land, and local ecosystems. The regression analysis shows a consistent negative correlation between LST and NDVI in the ALM from 1989 to 2019, with the correlation between vegetation and surface temperature increasing since 2019. The SAVI indicates a slight improvement in overall average vegetation health from 0.18 in 1989 to 0.25 in 2009, but a slight decrease to 0.21 in 2019. The SPI at 12 and 24 months indicates that drought severely impacted vegetation cover from 2014 to 2019, with notable recovery during improved wet periods in 1993, 2000, 2003, 2006, 2008, and 2013, possibly due to temporary drought relief. The findings can guide provincial drought monitoring and early warning programs, enhancing drought resilience, productivity, and sustainable livelihoods, especially in farming communities.

**Keywords:** agricultural drought monitoring; interdecadal variation; LST; NDVI; SAVI



**Citation:** Mbuqwa, P.; Magagula, H.B.; Kalumba, A.M.; Afuye, G.A. Interdecadal Variations in Agricultural Drought Monitoring Using Land Surface Temperature and Vegetation Indices: A Case of the Amahlathi Local Municipality in South Africa. *Sustainability* **2024**, *16*, 8125. https://doi.org/10.3390/su16188125

Academic Editors: Mariusz Sojka and Dariusz Młyński

Received: 7 July 2024
Revised: 5 September 2024
Accepted: 12 September 2024
Published: 18 September 2024



## 1. Introduction

Climate change causes severe weather events like droughts and changes in precipitation patterns, significantly impacting agricultural production, economic sectors, and vulnerable communities [1,2]. El Niño-Southern Oscillation (ENSO) phenomena primarily trigger drought globally in most arid and semi-arid regions [3]. Climate change is predicted to worsen drought, increasing the aerial extent of drought-affected areas, and potentially causing adverse effects on agriculture [4,5]. Droughts are classified into meteorological, agricultural, hydrological, and socioeconomic types, with their severity influenced by intensity, duration, spatial coverage, and local socioeconomic level, and exacerbated by global warming [6]. Drought poses significant challenges to environmental components and sustainable

human livelihoods due to its detrimental effects on agricultural activities [7]. Agricultural drought, a severe natural disaster causing crop productivity to decrease due to irregular rainfall and soil moisture, significantly impacts the economy, ecosystem, reservoirs, and water dam levels [8,9]. The Food and Agricultural Organization (FAO) accentuates that global drought has decreased food production and has increased food costs and malnutrition among its inhabitants [10]. The drought has led to land degradation and soil erosion, particularly severe in areas with the potential for agriculture. The growing global population demand for food production has prompted a focus on monitoring drought effects on agriculture to enhance ecosystem services and achieve sustainable development goals.

Agricultural drought monitoring uses various indices such as the normalized difference vegetation index (NDVI) [11], soil-adjusted vegetation index (SAVI) [12], and standardized precipitation index (SPI) [13] to evaluate the duration and severity of drought impacts [14]. The World Meteorological Organization (WMO) has confirmed the standardized precipitation index (SPI), developed by McKee et al. [14], for monitoring agricultural drought conditions using precipitation data across various timescales. Between 2012 and 2015, California experienced low precipitation and dry conditions, accelerating evapotranspiration and decreasing soil moisture, thereby worsening vegetation health [15]. The Lower Mekong Basin in Asia has experienced consistent droughts for 45 years, primarily during the dry season, causing water shortages for rice and upland crop production, with the most recent drought occurring in 2003 [16]. Numerous studies in China have utilised the NDVI to analyse agricultural drought, revealing its versatility on local, regional, and global scales [16,17]. A complex correlation was found between vegetation condition and precipitation, which has not been adequately studied using LST, SAVI, NDVI, and SPI, affecting drought index strengths [16]. According to the SPI drought class, a study on El Niño impacts in Southern Africa found that Zimbabwe experienced the most severe drought-prone period between 1991 and 1992 [18]. Moreover, a study used MODIS and NDVI data to analyse Zimbabwe's agricultural drought, identifying it as a key indicator for categorising the situation [19]. Another study utilised image differencing to generate a radiant temperature change image using the normalization of LST, to understand the impacts of land cover changes on climate trends [20]. Remote sensing technologies like unmanned aerial vehicles (UAVs) are utilised to bridge the gap between spaceborne and field observations, providing high-resolution remote sensing data for understanding drought conditions [21,22]. For instance, UAVs are used in research to monitor turfgrass phenotyping, improve agricultural production through smart farming and precision agriculture, and evaluate water-saving irrigation practices [23,24].

In South Africa, a study discovered that South Africa's high water reliance makes it highly susceptible to drought, with the highest risk for irrigated crops in Limpopo and Eastern Cape, and extreme droughts for rainfed croplands in Northern Cape, North West, and Limpopo [25]. The Palmer drought severity index (PDSI) indicates moderate impacts on precipitation, evapotranspiration, and soil moisture, with worsening drought conditions in the Western Cape Province between 2015 and 2019 [26]. The soil moisture drought index (SMDI) in Mediterranean South Africa revealed severe drought between 2015 and 2018, primarily due to autumn shortfalls and drier summer conditions [27]. Between 2015 and 2018, Cape Town in the Western Cape experienced severe drought, causing drier autumn conditions, crop reductions, and job losses in the agricultural sector due to a southward shift in storm tracks [28]. Similarly, droughts in northeast KwaZulu-Natal, particularly in the oldest proclaimed game reserve, Hluhluwe-iMfolozi Park, have caused frequent damage to vegetation, water, and wildlife resources [29]. Few scholars have evaluated the relationships between NDVI, SAVI, LST, and SPI in remote sensing drought-related impacts in South Africa at different timescales [2,25–29]. Hence, a comprehensive empirical analysis of each index becomes crucial for the current study.

South Africa's agricultural potential areas, particularly the Amahlathi Local Municipality (ALM) in the Northern Amathole District, are underrepresented in drought assessments, as drought significantly impacts food production and government grain reserves [30,31].

The ALM's warm temperatures and high annual rainfall of 495 mm, slightly above the country's average, increase vulnerability to drought, causing a significant decline in crop and livestock productivity among small-scale farmers [32]. For instance, the ALM is facing severe drought-related weather changes, causing severe temperature changes, and crop and livestock destruction due to decreased precipitation, soil moisture, wildfire frequency, altered wind patterns, and water depletion [33–35]. This study used a GIS-based weighted overlay, Pearson's correlation analysis, and multiple linear regression models to assess the correlations between LST, NDVI, SAVI, and SPI in response to agricultural drought from 1989 to 2019 [12,34,36]. Hence, comparing NDVI, LST, SAVI, and SPI is crucial for understanding their similarities and discrepancies in characterising, agricultural drought trends across the ALM. This study aims to employ remotely sensed LST, SAVI, NDVI, and SPI to assess interdecadal drought severity and duration in Amahlathi's agricultural potential zone from 1989 to 2019. The outcomes of this study can improve the understanding of microclimate dynamics in agricultural potential areas, and the relationships between drought indices and land cover distribution.

## 2. Materials and Methods

### *2.1. Study Area*

The Amahlathi Local Municipality (ALM) is located in the Northern part of the Amathole District Municipality in the Eastern Cape Province of South Africa (Figure 1a). The ALM is located between longitude and latitude 32°52′26″ S and 27°26′76″ E with an elevation of 1209 m (3967 ft). The total area covers an extent of 4820 km$^2$, which is dominated by a black population of 115,703 [36]. The region is bordered by the Chris Hani District Municipality to the north and the Buffalo City Metropolitan Municipality to the south, an administrative area and one of six municipalities, encompassing small towns like Tsomo, Cathcart, Keiskammahoek, and Stutterheim [37]. The Keiskammahoek area is renowned for its ecotourism and agricultural potential and faces challenges due to inequitable land management practices and complex tenure arrangements [37]. The ALM is characterised by warm average temperatures, typically ranging from 24 °C to 30° C and receiving 600 mm annual rainfall, heavily relying on the Sandile Dam as its primary water source due to its semi-arid conditions [36,37]. Consequently, the agricultural potential zones and land cover types have witnessed an increasing frequency, severity, duration, and spatial extent of long-term agricultural droughts in the Eastern Cape [36,37], requiring urgent attention for sustainability. Drought episodes impact processes in the ALM, affecting four biomes: Albany Thicket, Grasslands, Savannah, and Forest, affecting associated processes [37].

#### 2.1.1. Satellite-Derived Datasets

The study utilised Landsat imagery to monitor interdecadal variations in agricultural drought from 1989, 1999, 2009, and 2019 to estimate land surface temperatures and identify vegetation patterns related to drought dynamics. The satellite imagery was obtained from the United States Geological Survey (USGS) website (http//earthexplorer.usgs.gov/, accessed on 7 July 2024). Surface reflectance images from December to February were processed, mosaicked, and geometrically corrected to the World Geodetic System (WGS84) coordinate systems [38]. The study utilised Landsat bands in an arrangement of band 2, band 3, band 4, and band 5 based on their characteristics. Consequently, the Landsat TM and ETM+ images were interpreted using band combinations 4/3/2, while Landsat OL/TIRS images were interpreted using band combinations 5/4/3, as per Afuye et al. [39]. Landsat images were chosen for their superior temporal coverage, spatial and spectral resolution, and 30 m spatial resolution [38,39]. The selection of satellite imagery with minimal cloud coverage was made to minimise the impact of cloud coverage and emphasise the significance of seasonality in remote sensing [39,40].

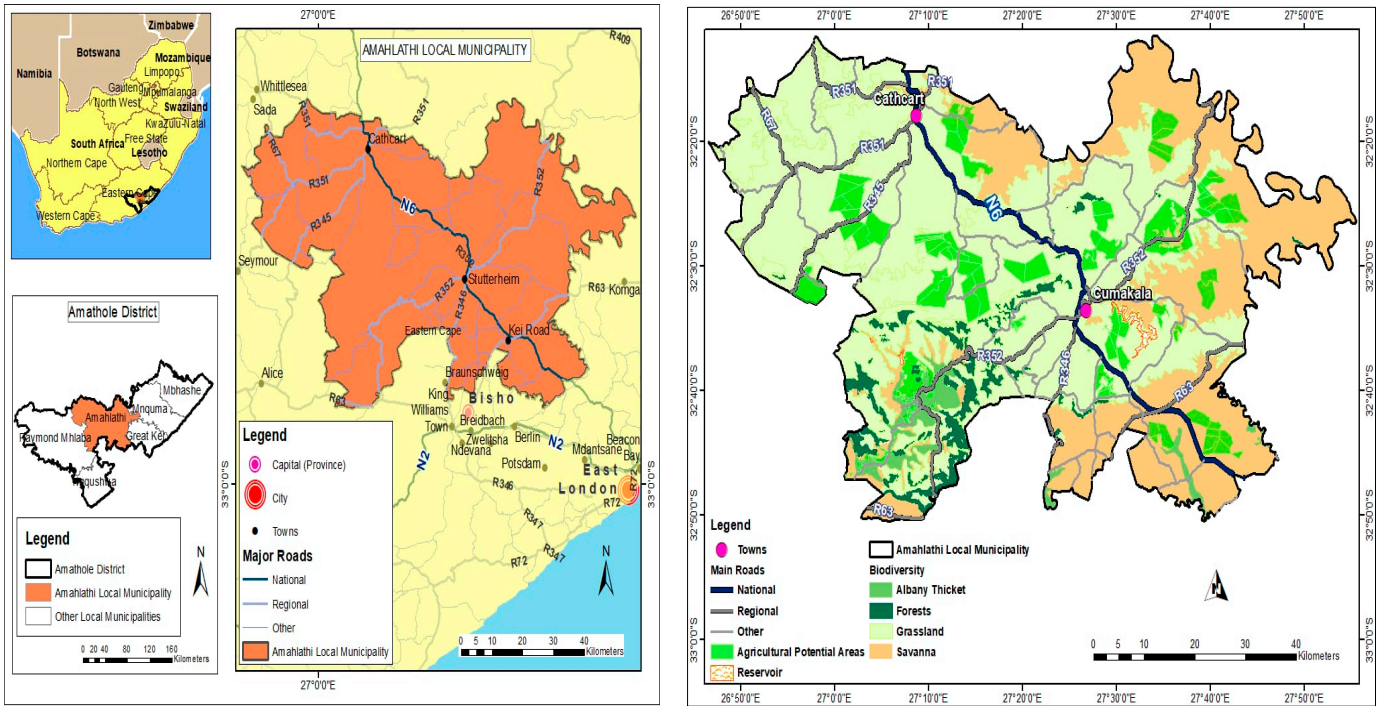


(**a**) (**b**)

**Figure 1.** (**a**) Map of the Amahlathi Local Municipality and (**b**) the distribution of land cover in agricultural potential zones in the Eastern Cape Province, South Africa.

#### 2.1.2. South African National Land Cover Classification Map

Land cover data for the Amahlathi Local Municipality (ALM) were obtained from the South African National Land Cover (https://egis.environment.gov.za/data_egis/data_download/current, accessed on 7 July 2024) from 1990 to 2020. The South African National Land Cover (SANLC) shows different biodiversity zones, including Albany thicket (light brown), forests (dark green), grassland (light green), and Savannah (pale orange), with each zone dominating different areas (Figure 1b). Albany thicket covers the northeastern and southern areas, while forests are scattered throughout the central and southern parts. Grassland is widespread across the municipality, while savanna is also found in patches in the northeastern and southeastern regions. The SANLC data were reclassified to evaluate vegetation stress and land cover distribution in agricultural potential zones, and its impact on agricultural areas [41,42]. The ALM vegetation classifications were reclassified based on land cover types like Albany thicket, forests, grassland, and savannah, and their distribution in agricultural potential zones (Figure 1b). Consequently, the study area was identified by importing a vector file from the municipal demarcation board into ArcGIS 10.7 software and clipping the larger Landsat scene to the ALM boundary. The reclassification of land cover types in the localized region's biodiversity was conducted to redress species of different vegetation classifications and detect changes [37,41]. Table 1a categorises agricultural drought severity based on images with less than 10% cloud cover. The larger imageries were reduced by clipping or sub-setting, which involves separating the preferred study area from the larger image into a smaller file for faster processing [42]. The dryness threshold, as described by McKee et al.'s [14] SPI values, indicates wetter conditions with values greater than 0 and dry conditions with negative values, as shown in Table 1b.

**Table 1.** (**a**,**b**) Drought severity classification of SPI values.

| (**a**) | |
|---|---|
| **SPI Value** | **Category** |
| 2.00 and above | Extremely wet |
| 1.50–1.99 | Very wet |
| 1.00–1.49 | Moderately wet |
| 0.99 to −0.99 | Near-normal |
| −1.00 to −1.49 | Moderately dry |
| −1.50 to 1.99 | Severely dry |
| −2.00 and less | Extremely dry |

| (**b**) | | |
|---|---|---|
| **Vegetation Category** | **NDVI and SAVI Range** | **Drought Severity** |
| No vegetation | <0.1 | Extremely dry |
| Low | 0.11–0.20 | Dry |
| Normal | 0.21–0.40 | Moderate |
| High | 0.41–0.60 | Wet |
| Very high | ≥0.61–1.00 | Extremely wet |

### *2.2. Study Methods*

The study employs multi-source remote sensing imagery and comparative analysis to evaluate the agricultural drought response to vegetation indices and land surface temperature (LST) at different time intervals in the study area. Landsat data were used to monitor interdecadal variations in agricultural drought from 1989, 1999, 2009, and 2019, estimating LST and detecting vegetation patterns. Vegetation indices estimate above-ground vegetation cover from remotely sensed products based on 10-year grouping were used to determine the changes between vegetation classes over time [2,39]. The normalized difference vegetation index (NDVI) is a broadly used index for identifying agricultural drought areas, with values ranging from −1 to +1 [40,42]. The NDVI was created for the years 1989, 1999, 2009, and 2019 from the band reflectance data, as computed in Equation (1).

$$\mathrm{NDVI} = \frac{(\mathrm{NIR} - \mathrm{RED})}{(\mathrm{NIR} + \mathrm{RED})} \quad (1)$$

where, NIR represents the near-infrared reflected by vegetation and RED is the red band absorbed by the chlorophyll found in vegetation [39]. The NDVI measures vegetation health by analysing the reflectance/radiation in the red and near-infrared bands. Moreover, the soil-adjusted vegetation index (SAVI) was used for its superior ability to differentiate between vegetation and soil in low-vegetation areas, making it suitable for both arid and semi-arid environments [43,44]. The multi-temporal analysis of SAVI was assessed by taking into account temporal variations in vegetation density over the years to derive the index using Equation (2).

$$\mathrm{SAVI} = \frac{(\mathrm{NIR} - \mathrm{Red})}{(\mathrm{NIR} + \mathrm{Red} + \mathrm{L})} \times (1 + \mathrm{L}) \quad (2)$$

where, the Red and NIR are the spectral reflectance of vegetation in the red and the near-infrared bands, respectively, and L is the soil brightness correction factor. Consequently, the extraction of the land surface temperature (LST) was carried out in the following phases: The digital number (DN) of the Landsat TM thermal infrared band was converted into spectral radiance using specific gain and bias values for each scene, resulting in the extraction of LST. Radiometric calibration was performed to extract brightness temperatures

and remove sensor errors [39], transforming DN values data into a meaningful radiometric scale using Equation (3).

$$L_\lambda = \frac{(L_{max\lambda} - L_{min\lambda})}{(Q_{Calmax} - Q_{Calmin})} (Q_{cal} - Q_{calmin}) + L_{min\lambda} \quad (3)$$

where, $L_\lambda$ is the spectral radiance at the sensor's aperture [W/(m$^2$sr μm)], $Q_{cal}$ is the quantized calibrated pixel value [DN], $Q_{Calmin}$ is the minimum quantized calibrated pixel value corresponding to $L_{min\lambda}$ [DN] = 1, Qcalmax is the maximum quantized calibrated pixel value corresponding to $L_{max\lambda}$ [DN] = 255, $L_{min\lambda}$ is spectral at sensor radiance that is scaled to *Qcalmin* [W/(m$^2$sr μm)], $L_{max\lambda}$ is spectral at sensor radiance that is scaled $Q_{Calmax}$ [W/(m$^2$sr μm)], Grescale is the band-specific rescaling gain factor [(W/(m$^2$sr μm))/DN], and Brescale is the band-specific rescaling bias factor [W/(m$^2$sr μm)]. Conversion from radiance to surface/brightness temperature [39]: the retrieved spectral radiance values were converted to a brightness temperature value by applying the inverse of Planck's function [45] using Equation (4).

$$T_B = \frac{K_2}{\ln\left(\frac{K_1}{L_\lambda} + 1\right)} \quad (4)$$

where, $T_B$ is the effective at-sensor surface/brightness temperature [$K$], $K_2$ is the calibration constant 2 [$K$], $K_1$ is the calibration constant 1 [W/(m$^2$sr μm)], $L_\lambda$ is the spectral radiance at the sensor's aperture [W/(m$^2$sr μm)], and ln is the natural logarithm. Finally, the temperatures were converted from Kelvin to degrees Celsius by subtracting 273.15 from the Kelvin to Celsius conversion rate.

#### 2.2.1. Weighted Overlay, Multiple Linear Regression Model and Correlation Analysis

The study used a 10-year grouping to analyse spatial variability in agricultural drought trends and severity classifications, utilising multiple linear regression (MLR) models from the ordinary least squares tool [36]. The GIS-based weighted overlay technique calculated the mean NDVI, SAVI, and LST, categorising drought themes into five classes: severe, heavy, moderate, mild, and no drought [39]. The annual drought classification map employs an equally weighted sum overlay analysis to categorise vegetation response to agricultural drought, reclassifying vegetation indices and LST changes over multiple years [34,35,42]. The method provides a global, non-spatial, and quantitative analysis of the linear relationship between LST as a dependent variable and NDVI, SAVI, and SPI as independent variables [34,44]. The model consists of LST as the independent variable and NDVI, SAVI, and SPI as the dependent variables, with the strength of the correlation and relationship between the variables determined by the $R^2$ value from the regression analysis [43]. The $R^2$ value ranges from 0.0 to 1.0, with a value of 1.0 indicating a strong correlation at all points. Conversely, an $R^2$ value of 0.0 means no correlation or linear relationship between X and Y [44]. The MLR modes were used to assess the impact of vegetation indices on land surface temperature at various time intervals, using Equation (5).

$$y_i = \beta_0 + \beta_1 x_{1i} + \beta_2 x_{2i} + \beta_3 x_{3i} + \ldots. + \beta_k x_{ki} + \varepsilon_i \quad (5)$$

where, $y_i$ is the dependent variable, which is a function of the linear combination of the independent variables $x_{ki}$, $\beta_0$ is the intercept, $\beta_k$ is the regression coefficient for the independent variable, and $\varepsilon_i$ is a normally distributed independent random error with constant variance. The pixel-wise Pearson's correlation analysis was used to determine the long-term trends and extent of agricultural drought in response to vegetation indices and land surface temperature at various time intervals [34,36,39,46]. The study used Pearson's correlation analysis to assess the relationship between LST, NDVI, SAVI, and

SPI in response to the agricultural drought extent from 1989 to 2019. Pearson's correlation coefficient analysis ($r_{xy}$) is computed using Equation (6).

$$r_{xy} = \frac{\sum_i (x_i - \overline{x})(y_i - \overline{y})}{\sqrt{\sum_i (x_i - \overline{x})^2 - \sum (y_i - \overline{y})^2}} \quad (6)$$

where, $x_i$ and $y_i$ are independent and dependent variables, respectively, and $x$ and $y$ are mean values of the samples ranging from $-1$ to 1.

2.2.2. Drought Characterization Based on Standardized Precipitation Index

The SPI was utilised to monitor agricultural drought in the ALM from 1989 to 2019 based on annual average precipitation data from the Application for Extracting and Exploring Analysis Ready Samples (AppEEARS) and retrieved from the National Aeronautics and Space Administration (NASA): Prediction of Worldwide Energy Resource Database (https://power.larc.nasa.gov/data-access-viewer/, accessed on 7 July 2024). Therefore, the data were used to calculate and quantify precipitation deficit at various timescales. The SPI computation uses precipitation as the sole hydrological input, with negative values indicating drought and positive values indicating wet conditions [47,48]. The study used McKee et al.'s [14] procedural approach to calculate the SPI time series for the ALM at 12-month accumulation periods using the Drought Indices Calculator (DrinC v1.7.97) software for data manipulation. Therefore, the DrinC (v1.7.97) software was utilised for evaluating drought indices based on meteorological, hydrological, and agricultural monitoring, enabling easy interpretation and strategic planning in various applications [49–51]. The SPI was calculated by dividing the difference between significant rainfall ($x_i$) and average rainfall ($x_m$) by the standard deviation ($\sigma$) of the selected period using the XLSTAT engine in Microsoft Excel v.4.2. The formula for calculating SPI is given by Equation (7).

$$\text{SPI} = \frac{X_i - X_m}{\sigma} \quad (7)$$

where, $x_i$ is the recorded rainfall by the weather station, $x_m$ is the average rainfall, and $\sigma$ is the standard deviation.

## 3. Results and Discussion

### *3.1. Spatiotemporal Dynamics of Interdecadal NDVI Trend*

Figure 2 shows the spatial distribution of NDVI values between 1989 and 2019, with the lowest values observed in the northwestern areas of the ALM. In 1999, the quality of green vegetation decreased in the northwestern and northeastern parts of the municipality. The development may be linked to the adverse effects of the El Niño-Southern Oscillation experienced across South Africa between 1989 and 1999 [3,39,52]. A previous study accentuated that the intensity and degree of extreme drought events may be directly linked to El Niño events [3]. In 2009, the northeastern and southeastern parts of the municipality experienced an increase in green vegetation distribution, with patches of stressed vegetation present. A previous study revealed that different vegetation patches are influenced by environmental factors like forest fires, high temperatures, rainfall deficiency, and human disturbances [35,48]. Likewise, the study area's vegetation status could have been influenced by related factors. In 2019, vegetation cover distribution and greening trend increased, with the maximum NDVI increasing in a trend from 0.82 to 0.94, indicating a 0.12% increase from 2009 (Figure 2). The variation in rainfall and rising temperature may have impacted vegetation growth and development in this area [4,53]. The minimum NDVI values consistently show $-1$ for 1989, 1999, and 2019, indicating areas with poor vegetation or exposed soil, with the 2009 value slightly higher at $-0.46$, as shown in Table 2. The highest NDVI values were consistently at the upper limit of 1 for 1989 and 1999, indicating areas with very high vegetation health. In 2009, the maximum NDVI value was slightly lower at 0.82, indicating less vegetation health. The mean NDVI values indicate the average

vegetation health, which decreased from 0.37 in 1989 to 0.32 in 1999, then increased to 0.42 in 2009, slightly decreasing to 0.39 in 2019. The standard deviation in NDVI values showed a significant increase from 0.12 in 1989 to 0.14 in 1999, indicating more variation in vegetation health. It remained consistent at 0.12 in 2009 and increased to 0.16 in 2019, indicating greater heterogeneity in vegetation health (Table 2). The NDVI values, with a mean of 0.39, suggest a high prevalence of drought conditions, consistent with previous studies indicating persistent droughts [39,41,54,55]. The results reveal the variability and improvement or decline in vegetation health across the region, providing a comprehensive understanding of vegetation changes in the study area.

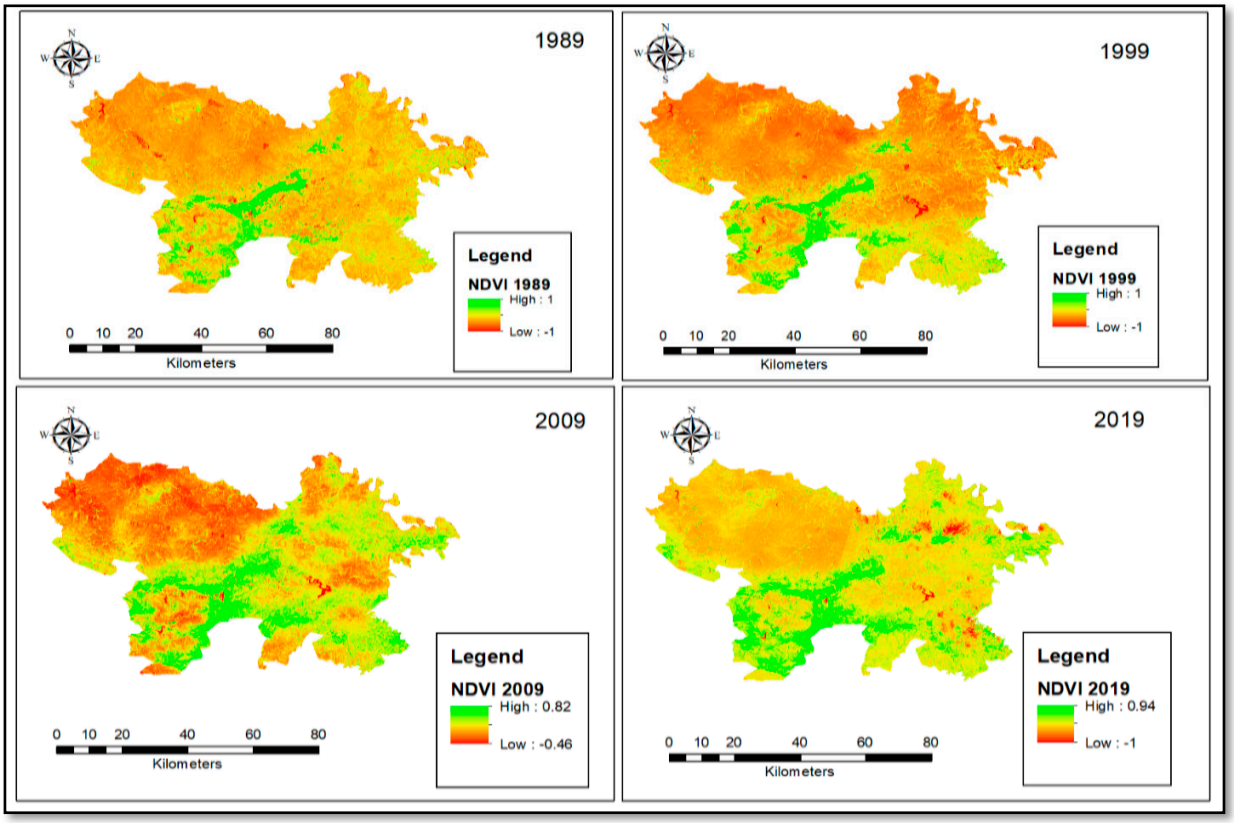


**Figure 2.** Spatiotemporal analysis of NDVI from 1989 to 2019.

**Table 2.** Normalized difference vegetation index (NDVI) from 1989 to 2019.

| Statistics | NDVI (1989) | NDVI (1999) | NDVI (2009) | NDVI (2019) |
|---|---|---|---|---|
| Min | −1 | −1 | −0.46 | −1 |
| Max | 1 | 1 | 0.82 | 1 |
| Mean | 0.37 | 0.32 | 0.42 | 0.39 |
| Standard Deviation | 0.12 | 0.14 | 0.12 | 0.16 |

### *3.2. Spatiotemporal Dynamics of Interdecadal SAVI*

Figure 3 shows the spatial distribution of SAVI values from 1989 to 2019, with the lowest values observed in the northwestern area of the ALM due to vegetation decline in 1999. However, the northeast and northwestern regions were found to have low or unhealthy vegetation. The results indicate that northern regions are experiencing increased stress on vegetation due to irregular rainfall distribution and previous dry spells, making them vulnerable to dearth conditions. This may have influenced vegetation biomass recovery due to low rainfall and evapotranspiration rates, but the recorded low indicates browning trends, indicating a low SAVI value [39,44,55]. In 2019, the SAVI index showed a

slight recovery in vegetation conditions, possibly due to the strength and distribution of the greening trend in certain areas. Consequently, the minimum values have shown significant variation over time, with the lowest minimum in 1989 (−0.83) and the highest minimum in 2009 (−0.17), as shown in Figure 3. This suggests that some areas had poor vegetation health or soil exposure, particularly in 1989. The maximum values indicate the highest observed vegetation health. The highest maximum SAVI value was in 1989 (0.96), followed by 2019 (0.77). There was a noticeable decrease in maximum SAVI value in 1999 and 2009, indicating a reduction in the highest levels of vegetation health compared to 1989. The mean SAVI values indicate the overall average vegetation health, which increased from 0.18 in 1989 to 0.25 in 2009, indicating an improvement, but slightly decreased to 0.21 in 2019. The variability increased from 0.05 in 1989 to 0.07 in 2009 and 2019 (Table 3) This increase in standard deviation suggests that vegetation health became more heterogeneous over time, with a wider range of conditions observed across the region. By comparison, NDVI and SAVI variables show varying drought severity levels, with SAVI indicating drier conditions than NDVI, possibly due to the nature of the components in computing SAVI values [39]. A study indicates that the soil moisture factor, which considers plant and soil reflections, results in lower SAVI values compared to NDVI values [43]. Hence, the results highlight the dynamic nature of vegetation health and the importance of continuous monitoring for sustainable land management and environmental conservation. The region's vegetation health fluctuated with an improvement from 1989 to 1999, mixed results from 1999 to 2009, and a decline from 2009 to 2019, indicating potential environmental stressors or land use changes affecting the region.

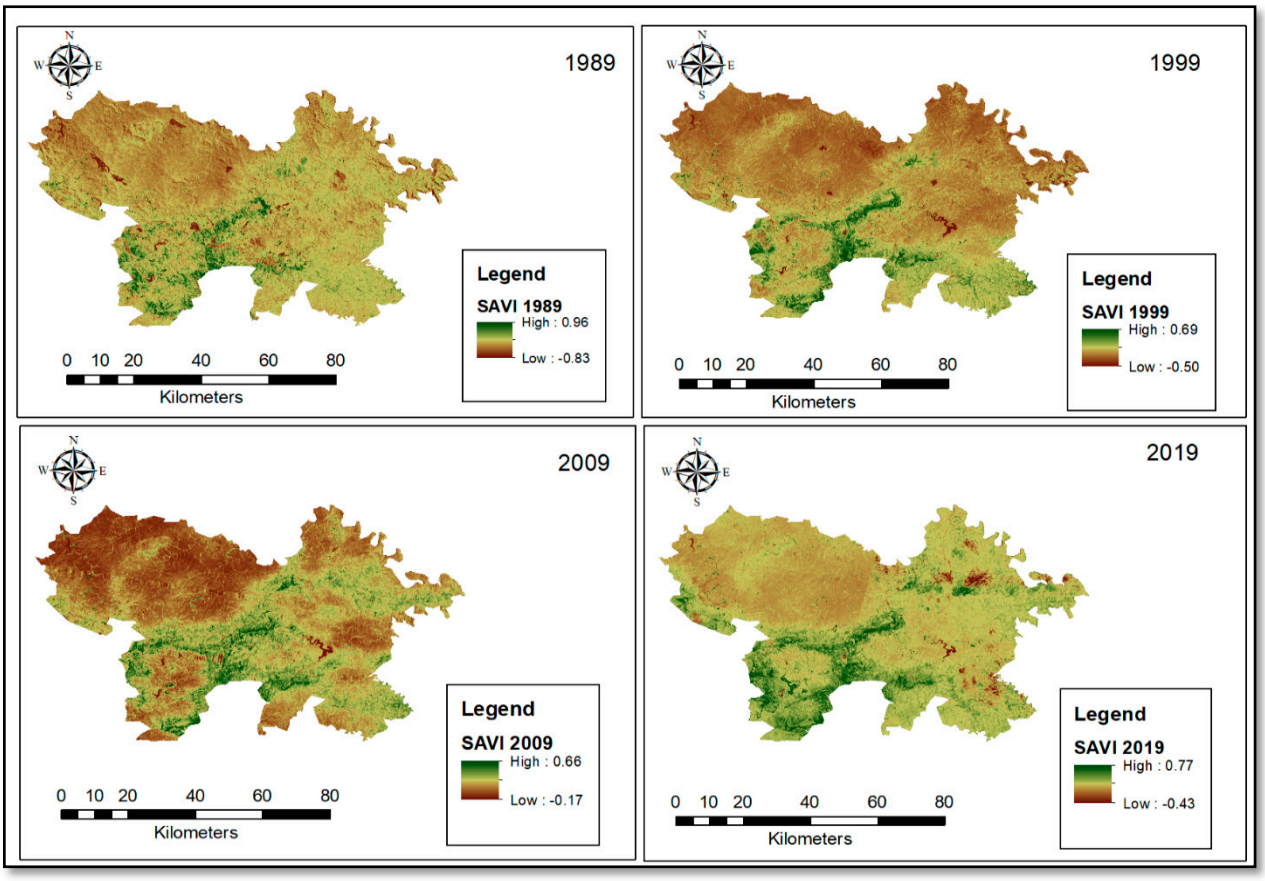


**Figure 3.** Spatiotemporal analysis of SAVI from 1989 to 2019.

**Table 3.** Soil-adjusted vegetation index (SAVI) from 1989 to 2019.

| Statistics | SAVI (1989) | SAVI (1999) | SAVI (2009) | SAVI (2019) |
|---|---|---|---|---|
| Min | –0.83 | –0.50 | –0.17 | –0.43 |
| Max | 0.96 | 0.69 | 0.66 | 0.77 |
| Mean | 0.18 | 0.16 | 0.25 | 0.21 |
| Standard Deviation | 0.05 | 0.06 | 0.07 | 0.07 |

### *3.3. Spatiotemporal Dynamics of Interdecadal LST*

Figure 4 shows the spatiotemporal analysis of land surface temperature (LST) from 1989 to 2019 in the ALM. The municipality experienced a relatively even distribution of low temperatures in 1989, while in 1999, there was a sharp increase in the distribution of low standard temperatures along the northeastern part. Between 2009 and 2019, the study area experienced a significant rise in high LST values in the northeastern and western areas, including the southeastern regions. The LST measures vegetation stress due to the effect of varying high temperatures, estimating the conditions [43,56], thus revealing different vegetation drought responses to temperature in the area. High-temperature values suggest moisture stress on soil and vegetation, suggesting that high surface thermal characteristics positively impact moisture stress on vegetation [56,57]. Unprecedented drought conditions in the ALM continue to threaten large areas due to negative soil and vegetation disturbances, causing devastating effects on agricultural production. Land surface temperature impacts soil moisture, which leads to an increased evaporative rate in semi-arid regions and vegetation cover, as per previous studies [27,35,41,43,58]. The minimum LST values show a general increase in baseline surface temperatures from 4.78 °C in 1989 to 16.01 °C in 1999 and 16.55 °C in 2009, with a slight decrease to 6.31 °C in 2019, indicating some cooler areas (Figure 4 and Table 4). The maximum LST values increased from 37.82 °C in 1989 to 40.03 °C in 1999, slightly decreasing to 38.89 °C in 2009, and then again to 40.12 °C in 2019, indicating generally higher peak temperatures. High temperatures have caused soil and vegetation to dry out, reducing nutrient levels and resulting in less productive soil for agricultural activities. The mean LST values significantly increased from 16.40 °C in 1989 to 33.55 °C in 1999, 34.67 °C in 2009, and slightly decreased to 29.91 °C in 2019, possibly due to land use, urbanisation, or climate patterns [59]. The standard deviation in surface temperatures increased from 2.32 °C in 1989 to 3.44 °C in 1999, 3.93 °C in 2009, and slightly decreased to 3.80 °C in 2019 (Table 4). This suggests a rise in surface temperature variability over time, indicating a greater diversity of temperature conditions across the landscape. Consequently, the increase in mean temperatures and variability highlights the impact of factors such as urbanisation, deforestation, and climate change on surface temperatures. The results of this study confirm previous findings that high LST values indicate severe drought susceptibility, while low LST values indicate minimal or no drought occurrence [60–62]. The Amahlathi Local Municipality's reduced vegetation may be due to climate change, affecting groundwater recharge due to excessive evaporation and land surface temperature changes [44,60,63].

**Table 4.** Land surface temperature (LST) statistics from 1989 to 2019.

| Statistics | LST °C (1989) | LST °C (1999) | LST °C (2009) | LST °C (2019) |
|---|---|---|---|---|
| Min | 4.78 | 16.01 | 16.55 | 6.31 |
| Max | 37.82 | 40.03 | 38.89 | 40.12 |
| Mean | 16.40 | 33.55 | 34.67 | 29.91 |
| Standard Deviation | 2.32 | 3.44 | 3.93 | 3.80 |

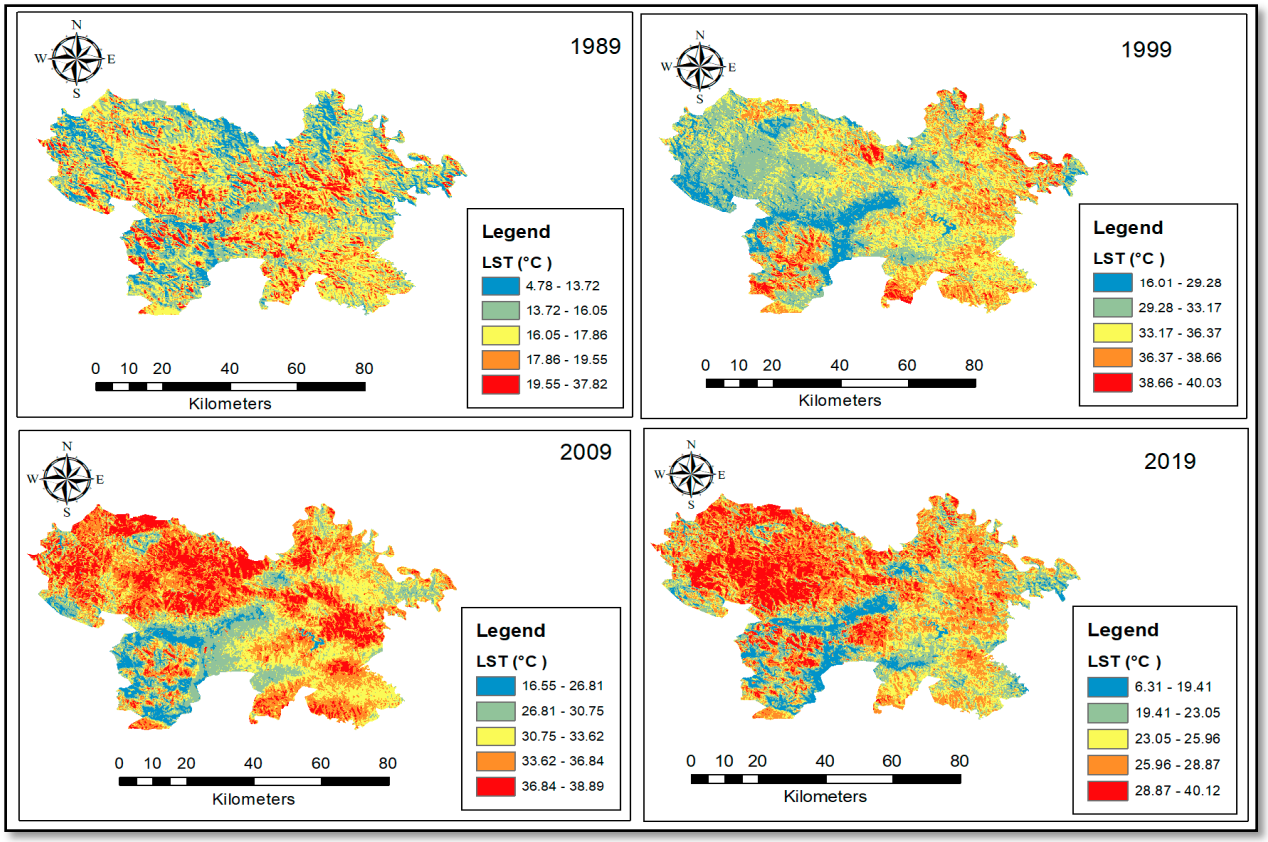


**Figure 4.** Spatiotemporal analysis of LST from 1989 to 2019.

### *3.4. Spatial Distribution of Interdecadal Variability of Drought in the ALM between 1989 and 2019*

Figure 5 shows the drought classification for the Amahlathi Local Municipality in South Africa from 1989 to 2019. The classifications of drought severity are based on a colour-coded legend, indicating levels of severe, heavy, moderate, mild, and no drought. The 1989 map shows moderate to heavy drought in a significant portion of the area, with some regions showing mild drought and limited areas showing no drought. The 1999 map shows moderate to heavy drought in the area, with an increase in mild drought cases compared to 1989, and few areas are drought-free. The 2009 map shows a slight improvement in drought areas, with more mild drought areas, moderate to heavy drought areas reduced, and no drought regions remaining limited. The 2019 map reveals a significant rise in severe drought areas, extensive heavy drought areas, and limited drought-free areas, indicating a worsening drought situation (Figure 5). From 1989 to 2019, drought severity increased significantly, with severe drought areas expanding significantly from their minimal levels in earlier years. Drought classifications have fluctuated over time, but the overall trend suggests an increase in drought conditions, consistent with negative SPI data in recent years, indicating prolonged dry conditions. For instance, prolonged droughts might have disrupted the biodiversity balance, leading to forest recession and expansion of savanna or grasslands into water-rich areas, affecting agricultural landscapes (Figure 1b). Studies show that drought effects vary spatially and over time, influenced by factors such as rainfall, climate, soil, topography, and vegetation type [46,62,63]. These factors affect water availability, agricultural productivity, and ecosystem health, resulting in varying vulnerability and resilience among regions and communities [64].

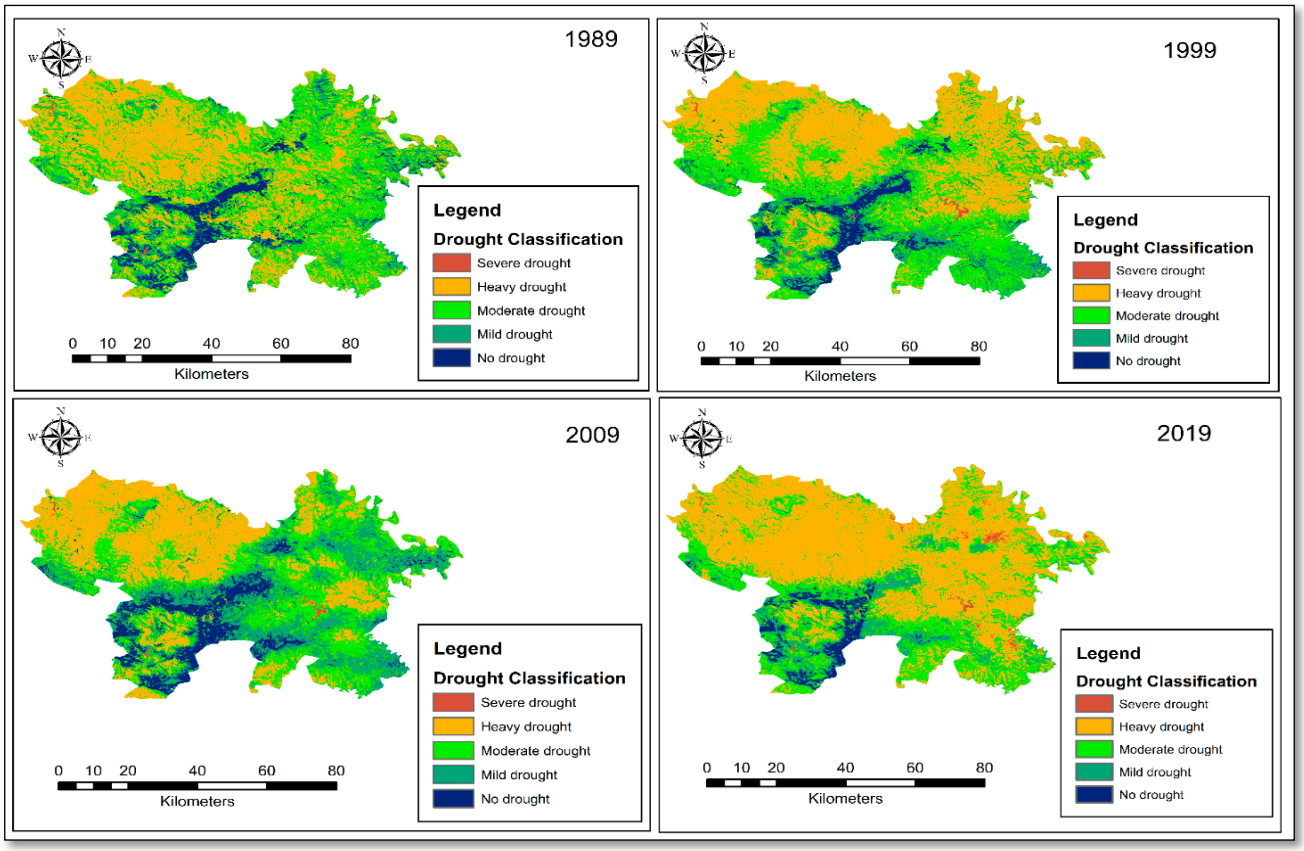


**Figure 5.** Drought classification for the ALM from 1989 to 2019.

The ALM experienced moderate to extreme drought in most areas, with a rising trend in dry spells, particularly in the northern part of the municipality, while the southern parts experienced mild to no drought conditions. The variation in these factors might have resulted in contrasting effects or heterogeneity of dryness in the municipality's northern and southern parts [39,60]. This highlights the need for region-specific strategies to manage water resources and agricultural practices and mitigate drought impacts effectively. Climate change has led to worsening drought conditions, affecting rainfall patterns and increasing temperatures, as evidenced by higher LST values. The increasing severity of droughts necessitates urgent adaptation measures to manage water resources effectively and promote sustainable agricultural practices. The results reveal a consistent increase in drought severity in the Amahlathi Local Municipality from 1989 to 2019. This trend emphasises the need for proactive measures to mitigate climate change's effects on water availability and agricultural productivity. The land cover map reveals grassland dominating the southwestern and central areas towards the east, while the savannah is found in the northeastern and southern parts of the municipality (Figure 1b). This connotes that the agricultural potential zones in the ALM exhibit a patchy pattern due to soil types, vegetation, and water access, which are impacted by drought conditions, making some areas less viable for agriculture. The Albany thicket was primarily found in the central and southeastern regions, with the forests appearing least in the southern areas. The results indicate that drought impacts agricultural areas by reducing soil moisture, hindering plant growth, leading to crop failures, and affecting plant physiological processes and yield. As a result, drought-induced reductions in water levels near reservoirs or major rivers might have potentially affected irrigation and crop yields.

Table 5 shows data on drought classification from 1989 to 2019, revealing affected areas (4380 km$^2$) under different drought conditions in the ALM. The study categorised drought classes by spatial distribution, with severe drought covering 9 to 38 km$^2$ of the

area, with an average coverage of 18.2 km$^2$ for the study period (Tables 1a and 5). In 2019, the severe drought area experienced a significant increase of 0.9% compared to previous years (0.2–0.3%) as shown in Table 5. Extreme drought in the area is increasing, with a significant spike in 2019 (55.8%), indicating worsening conditions over time, with the lowest percentage in 2009 (31.6%). However, the extreme drought condition increased from 35.4% in 1989 to 40.0% in 2009, then decreased to 31% in 2009 and significantly increased in 2019 to 55.8%, equivalent to 2446 km$^2$ in area extent. The region, covering approximately 40% of the area, is dominated by moderate to extreme drought classes, which are prevalent during the study period, covering 1.698 km$^2$. The moderate drought areas decreased from 43.0% in 1989 to 29.6% in 2019, suggesting that previously moderate drought regions may have transitioned to more severe drought categories. The area experienced a significant increase in mild drought in 2009 (24.1%), but a significant decrease in 2019 (9.9%). The percentage of drought-affected areas has consistently decreased, reaching its lowest percentage in 2019 at 3.8%, indicating an increasing extent of drought-affected areas (Table 5). For instance, studies discovered that moderate to extreme droughts in Kwazulu-Natal were witnessed between 2008 and 2018, causing significant developmental setbacks due to irregular rainfall distribution [40,57]. Consequently, the variations in rainfall distribution may have exacerbated climate change-exacerbated droughts in the ALM, potentially impacting food security, water availability, and vegetation distribution. The development may be linked to the area's microclimate dynamics, potentially causing severe low dams and river levels and potentially affecting agricultural production [2,25]. This connotes that large areas experience more complex and changeable climate characteristics due to significant variations in microscale climates and their impact on vegetation [8,39,60]. Overall, the results reveal that low and variable rainfall patterns significantly contribute to the persistence of dry spells in a municipality, with an average of 15.4% experiencing mild drought and 6.7% having no drought (Table 5). The 30-year drought severity trend has significantly increased, with extreme drought areas more than doubling from 1989 to 2019, indicating a worsening drought scenario. The NDVI and LST analyses reveal that the worsening drought conditions are attributed to various factors such as climate change, land use changes, and reduced vegetation cover [65]. The observations underscore the need for improved drought management strategies and adaptation measures to mitigate the negative impacts of severe and extreme drought conditions.

**Table 5.** Summary statistics results of the area covered by drought classes in the ALM.

| | **1989** | | **1999** | | **2009** | | **2019** | |
|---|---|---|---|---|---|---|---|---|
| **Drought Classification** | **Area (km$^2$)** | **%** | **Area (km$^2$)** | **%** | **Area (km$^2$)** | **%** | **Area (km$^2$)** | **%** |
| Severe drought | 9 | 0.2 | 13 | 0.3 | 12 | 0.3 | 38 | 0.9 |
| Extreme drought | 1552 | 35.4 | 1753 | 40.0 | 1382 | 31.6 | 2446 | 55.8 |
| Moderate drought | 1884 | 43.0 | 1747 | 39.8 | 1522 | 34.7 | 1296 | 29.6 |
| Mild drought | 608 | 13.9 | 592 | 13.5 | 1057 | 24.1 | 435 | 9.9 |
| No drought | 327 | 7.5 | 275 | 6.3 | 408 | 9.3 | 165 | 3.8 |

Figure 6 shows the correlation between LST and NDVI from 1989 to 2019 across the ALM. The results revealed a significant negative correlation between higher temperatures and lower NDVI values in areas with higher temperatures. Higher LST areas showed lower NDVI values, with a strong negative relationship and correlation coefficients of $R^2$ = 0.8758, 0.8879, 0.9639, and 0.9889, respectively. High temperatures can negatively impact vegetation health, affecting NDVI values and local temperatures in vegetated areas [39]. Consequently, vegetation stress can decrease transpiration and evapotranspiration, leading to higher temperatures and a feedback loop that further affects vegetation health [61,64]. The relationship between LST and NDVI ($R^2$ = 0.8758) is strongly negative, with a higher NDVI indicating increased vegetation density, leading to a decrease in LST in 1989 (Figure 6). The strong negative correlation ($R^2$ = 0.8879) in 1999 suggests that higher vegetation density is linked

to lower temperatures. In 2009, the negative correlation between high vegetation density and lower surface temperatures was stronger than in previous years, indicating a strong relationship. In 2019, NDVI and LST showed a consistent negative correlation ($R^2$ = 0.9889), with areas with higher vegetation density being significantly cooler. The negative correlation suggests an increase in vegetation density with a decrease in LST, aligning with similar findings in agricultural drought assessment [11,66–68]. The negative relationship across different years suggests a stable pattern where vegetation plays a crucial role in regulating land surface temperatures. The correlation between vegetation and surface temperature has become more pronounced or better detected over time, as evidenced by the increase in values since 2019. Overall, the results reveal a strong negative correlation between LST and NDVI, suggesting that areas with a higher vegetation density tend to have lower surface temperatures. The increasing relationship between vegetation cover and temperature may be influenced by climate change, as temperature variations pose significant ecological and economic risks [39,69]. The study emphasises the significance of efficient water management and cooling strategies in agriculture to mitigate the impact of high temperatures on crop health and ecosystem sustainability. Moreover, the impact of temperature on vegetation health underscores the need for effective management strategies in response to changing climatic conditions.

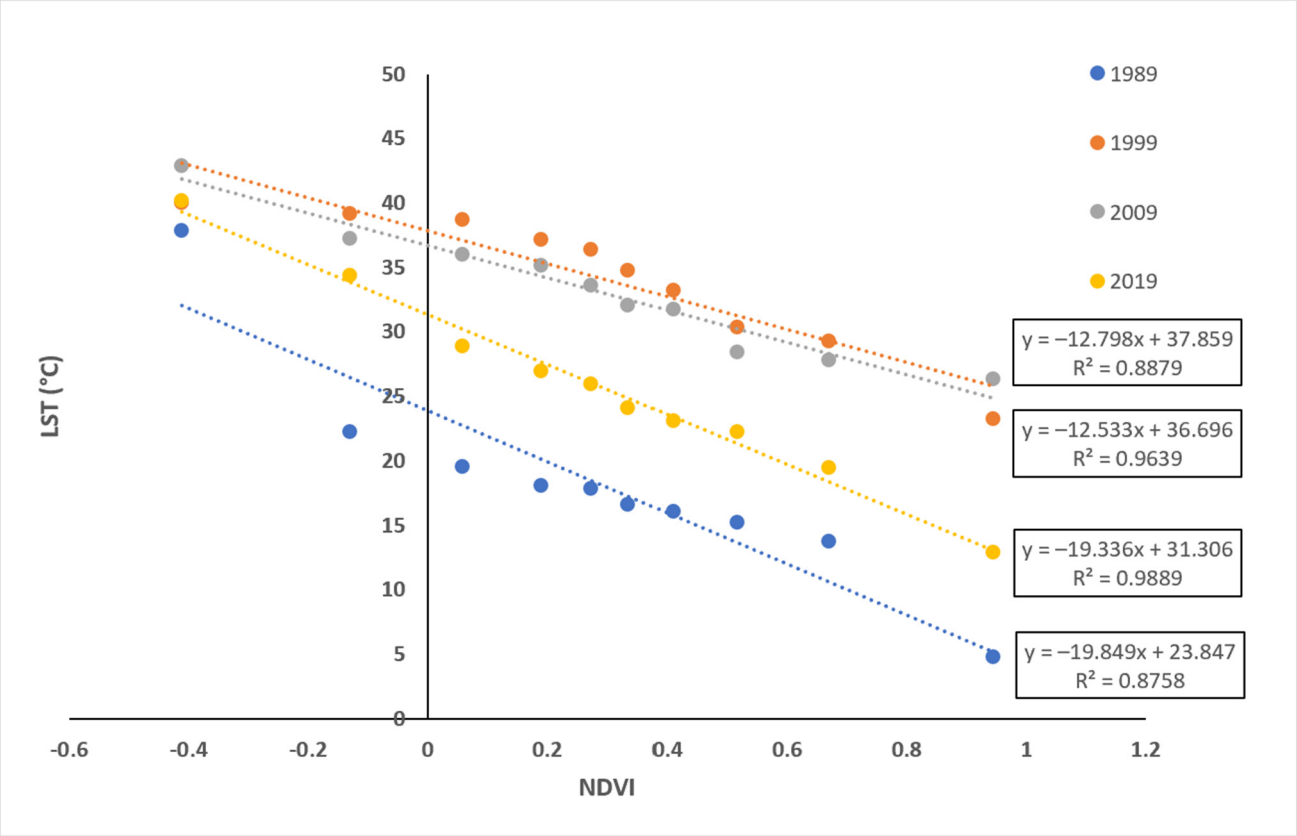


**Figure 6.** Correlation analysis between LST and NDVI from 1989 to 2019 in the ALM.

Figure 7 shows the correlation between LST and SAVI-derived vegetation fractions across the ALM. The correlation analysis revealed that surface temperature changes (LST) and vegetation health (SAVI) have an inverse relationship. The results show a significant negative correlation ($R^2$ = 0.8744) between LST and SAVI for 1989. The 1999 correlation ($R^2$ = 0.9643) strongly suggests that as SAVI increases, LST significantly decreases. In 2009, the correlation between the LST and SAVI was strong and negative, with a slightly weaker value ($R^2$ = 0.8527) compared to 1989 and 1999. The 2019 negative correlation ($R^2$ = 0.9643) is strong, with a high coefficient of determination, indicating a strong negative correlation

(Figure 7). The consistently high $R^2$ values for SAVI suggest strong negative correlations between SAVI and LST across all years. Due to its soil adjustment feature, SAVI consistently exhibits strong negative correlations across all years with LST, particularly in semi-arid environments. Previous studies have shown an inverse relationship between temperature and vegetation density, with increased temperature leading to decreased vegetation density [58,67,68,70]. The study indicates a moderately strong correlation between land surface temperature and vegetation health, with $R^2$ values ranging from 0.8527 to 0.9643. This suggests that the decline in vegetation density in the ALM may have been exacerbated by decreased soil moisture and rainfall patterns over time. The development may have disrupted crop development, causing insufficient water supply during crucial stages of planting and harvesting due to disrupted season timings [57,71]. The region's persistent dry spell, influenced by high temperatures and rainfall variability, could significantly affect vegetation cover, agricultural production, and the economy [39,44]. Consequently, drought-induced climate change in the ALM can significantly affect agricultural resources, food and water shortages, ecosystem functioning, and community resilience. Overall, the study shows a negative correlation between SAVI and LST, indicating that SAVI is more effective in assessing agricultural drought conditions in semi-arid environments with significant soil exposure. Provisional drought strategies are crucial for managing agricultural risks in the study area and ensuring food and water security in a changing climate.

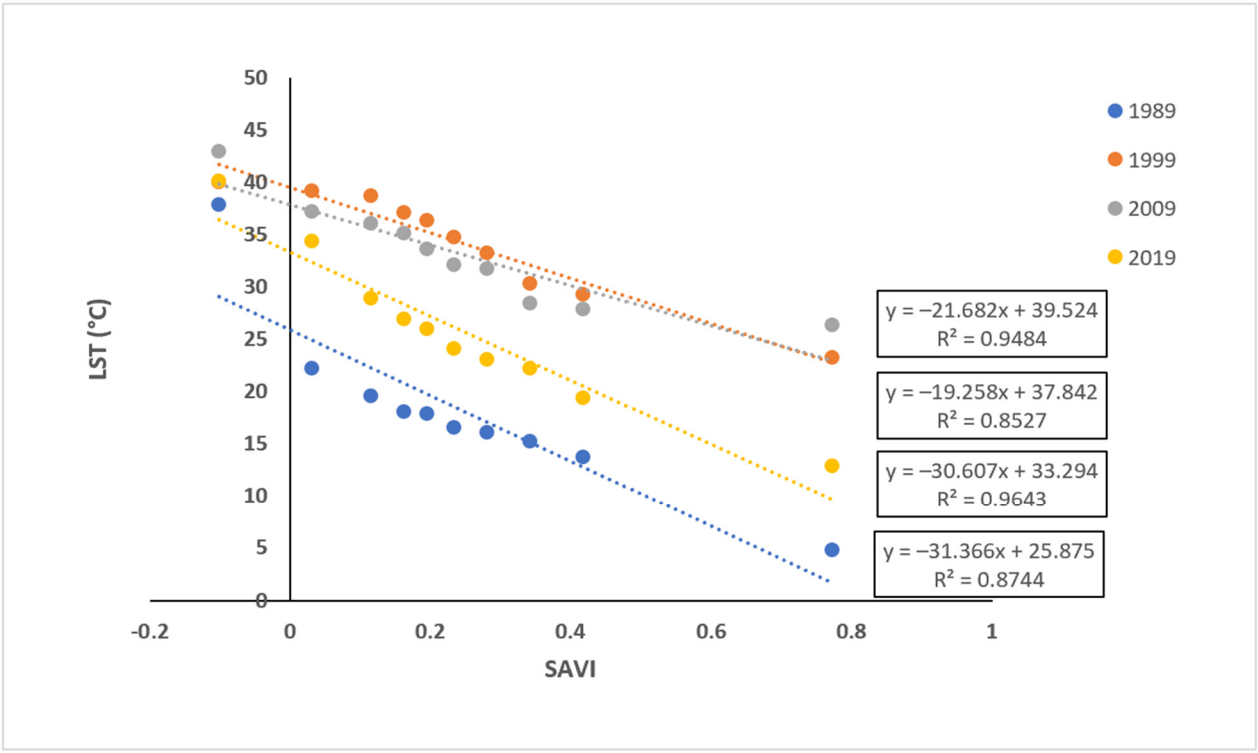


**Figure 7.** Correlation analysis between LST and SAVI from 1989 to 2019 in the ALM.

### *3.5. Standardized Precipitation Index Classification*

Figure 8 shows 12- and 24-month standardized precipitation index (SPI) drought patterns in the Amahlathi Local Municipality (ALM) from 1989 to 2019. The 12- and 24-month SPI scales are used to calculate agricultural drought by analysing long-term precipitation patterns using monthly average time series data, quantifying precipitation deficits and surpluses. The blue bars represent the 12-month SPI, indicating short-term drought or wet periods over a 1-year timescale while the orange bars represent the 24-month SPI, indicating longer-term drought or wet periods over a 2-year timescale. Consequently, the wet years show higher positive SPI values while the frequent drought years have lower negative SPI values. Although the SPI 12 and SPI 24 show similar trends, the SPI

12 magnitude may differ significantly, suggesting that shorter-term conditions may not always align with longer-term trends. The results revealed that certain years in the study area experienced a higher level of drought impact. The results of the 12- and 24-month SPI values for dry episodes range from −0.50 to −2.10, while wet episodes range from 1.00 to 2.00, causing significant impacts on vegetated ecosystems. The most drought-affected years were 1991–1992, 1993–1994, 1995–1996, and 1997–1999, with extended negative values observed between 2014 and 2019 (Figure 8 and Table 1a). During periods with reduced precipitation, the overall health of the ecosystem was affected, leading to a decrease in vegetation. Extreme agricultural droughts in the ALM occurred between 2016 and 2017, with consecutive negative SPI values from 2014 to 2019 indicating a prolonged drought period (Table 1a,b). According to the SPI classification results, the ALM experienced severe to extreme drought episodes from 2014 to 2019, primarily due to South Africa's strongest El Niño observed period [50,72]. By implication, the phenomenon led to a significant decrease in crop and livestock productivity among small-scale farmers in the local municipality [32,33]. The Eastern Cape province, particularly the study area, is experiencing extremely dry conditions, as confirmed by previous studies [39,50,60,72].

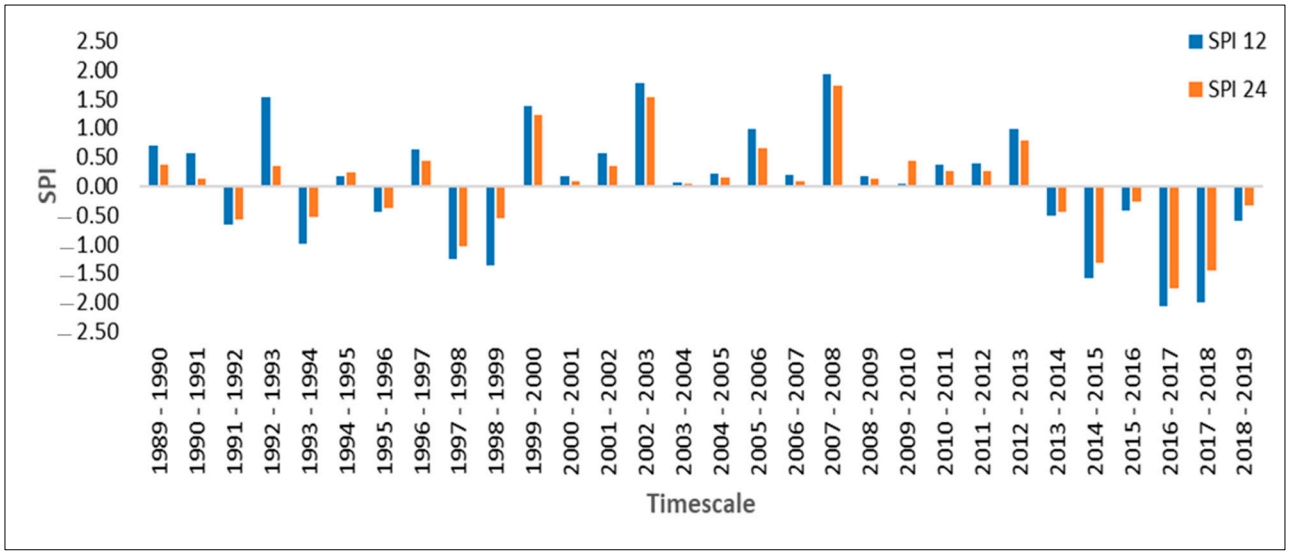


**Figure 8.** SPI drought patterns for 12 and 24 months in the ALM (1989–2019).

Droughts are predicted to increase in frequency and severity between 2030 and 2050, as evidenced by studies showing similar severity categories in remotely sensed products [50–52]. On the other hand, the study shows above-normal rainfall periods with positive SPI values in 1989–1991, 1992–1993, 1994–1995, 1996–1997, and 1999–2013, with notable positive SPI values in 1993, 2000, 2003, 2006, 2008, and 2013, respectively. These periods indicate wetter-than-normal conditions, which may have temporarily alleviated drought conditions. Over 30 years, a cyclical pattern of alternating wet and dry conditions has been observed, with severe droughts significantly impacting agriculture and livestock health [37,60,69]. Therefore, prolonged drought conditions between 2014 and 2019 have significantly impacted water availability, agricultural land, and the local ecosystem, with a concerning trend of predominantly negative SPI values, indicating an increasing frequency and severity of droughts. Overall, the SPI results reveal significant precipitation variability, with notable drought and wet periods which have implications for the ALM. The severity of droughts poses a significant threat to agricultural zones in the ALM, especially those with limited water resources or less drought-resistant vegetation [39,60]. The stress could lead to reduced crop yields, agricultural potential zone shifts, ecological impacts, and altered farming activities, posing negative implications for water resources management, climate adaptation, and environmental monitoring. The observed drought patterns in the ALM

highlight the need for proactive climate adaptation, involving improved water storage and distribution infrastructure, community drought-resistant practices, and effective integrated water resources management.

## 4. Intervention Strategies for Provincial Drought Monitoring and Policy Decision Support for Early Warning Systems

Despite significant advances in agricultural drought monitoring technologies and methods, several challenges remain. Innovative intervention strategies, such as the creation of provincial drought monitoring and early warning programs, are critical in mitigating the impacts of drought on agriculture and water resources. Consequently, these programs leverage advanced technologies like remote sensing, geographic information systems (GIS), and climate modelling to provide accurate and timely data on drought conditions [54,62,70]. By integrating LST and multimodal vegetation indices, these systems can detect early signs of water stress in crops and natural vegetation. Early warning systems can significantly mitigate the negative impacts of agricultural drought and other hazards by integrating scientific data into policy decision-making processes. Early warning programs inform farmers, policymakers, and communities about potential issues, enabling proactive measures like water conservation, crop rotation, and resource allocation. Policymakers should utilise analytical tools and timely data to predict, prepare for, and mitigate hazards like agricultural drought, providing actionable information to reduce risk and enhance resilience.

In regions like the Amahlathi's agricultural potential zone, South Africa, the impact on agriculture is profound, threatening the region's food security and economic stability. Prolonged droughts in the region reduce soil moisture, hindering crop growth and yields, particularly affecting staple crops like maize and wheat, crucial for local consumption and market supply. Water scarcity has exacerbated land degradation and soil erosion, reduced land productivity, and negatively impacted livestock farming, affecting pasture availability, animal health, and productivity, leading to reduced agricultural practices [30,33,37]. Consequently, socio-economic factors in Amahlathi exacerbate challenges faced by farmers, who rely on agriculture for their livelihoods, making them susceptible to the adverse effects of drought. The agricultural sector's cumulative impact leads to economic disruption, increased food prices, and increased food insecurity risk for the population [56,69,72]. To address these issues, comprehensive strategies involving improved data quality, robust policy frameworks, advanced water resource efficiency, long-term sustainability support of agricultural management systems, and capacity building are required. Amahlathi should strategically launch a large-scale food agricultural project, investing in infrastructure, land use management, and infrastructural support to boost the local economy. Innovative intervention strategies can enhance drought resilience, productivity, and sustainable livelihoods for farming communities in Amahlathi's agricultural potential zone. Integrating these innovative strategies can accurately predict the onset, cessation, duration, frequency, severity, and spatial extent of long-term agricultural droughts in any region. Therefore, innovative strategies improve resilience by enhancing preparedness, reducing vulnerability, and ensuring sustainable water resource management amidst changing climatic conditions.

### *Limitations and Future Perspectives*

The study utilised LST, NDVI, SAVI, and SPI to evaluate the extent and severity of agricultural drought conditions. Drought accuracy is influenced by changes in input datasets, uncertainties from data gaps, and temporal inconsistencies, which can impact drought assessments. The multiple linear regression model effectively identifies spatial variability in agricultural drought trends and severity classification, but its subjective continuous outcome variable may lead to biased estimates. Further research is needed to evaluate the effects of water-stressed vegetation on agricultural drought and predict the ENSO drought onset using the reservoir drought index (RDI) and climate change scenarios. This can assist in predicting long-term agricultural droughts at both local and regional scales. The study recommends a higher spatial resolution dataset for assessing agricultural

drought severity and a larger sample size for a stronger correlation between LST, hydro-meteorological factors, and vegetation indices. Consequently, a larger dataset or field-based observations are needed to improve the correlation between hydrological, meteorological, and agricultural drought under climate change scenarios. The study suggests further research on advanced statistical methods and machine learning algorithms for the fusion of UAV-based multi-sensor data to assess the impact of vegetation feedback on drought characteristics at different scales.

## 5. Conclusions

The study utilised remotely sensed LST, SAVI, NDVI and SPI to assess the interdecadal drought severity and duration in Amahlathi's agricultural potential zone from 1989 to 2019. The study reveals that the dryness in the northern and southern parts of the municipality is primarily influenced by factors such as decreasing precipitation. The study found that moderate to high agricultural drought conditions negatively impact vegetation change, with land surface temperature having the greatest influence on growth and distribution. The study reveals that LST accuracy in dry areas increased to 55.8% in 2019, despite dense vegetation and a high average temperature of 40.12 °C, impacting water availability, agricultural land, and local ecosystems. The regression analysis shows a consistent negative correlation between LST and NDVI in the ALM from 1989 to 2019, with the correlation between vegetation and surface temperature increasing since 2019. The study indicates a negative correlation between LST and NDVI, suggesting that increased vegetation density leads to lower surface temperatures, possibly due to atmospheric variation in vegetation changes. In addition, the study reveals a significant negative correlation between SAVI and LST, suggesting that SAVI is a more effective indicator for assessing agricultural drought conditions in semi-arid regions. The SPI indicates that drought severely impacted vegetation cover from 2014 to 2019, with notable recovery during improved wet periods in 1993, 2000, 2003, 2006, 2008, and 2013, possibly due to temporary drought relief.

Prolonged droughts in the ALM cause vegetation changes, biodiversity disruption, forest recession, and agricultural landscape expansion revealing patchy patterns in potential zones. The ALM drought dynamics case demonstrates that land cover distribution in agricultural potential zones is influenced by physical and climate-related factors. The findings provide valuable insights into the 12- and 24-month SPI-drought class between 1991 and 1999, revealing less frequent and longer-lasting episodes, particularly between 2015 and 2019. The study identifies high-risk areas for improvement in agricultural areas, providing data on drought incidences in rain-dependent agricultural areas, and enabling the precise creation of a drought prediction system and risk assessment program. The study suggests the need for enhanced monitoring, planning, awareness raising, and developing innovative strategies to mitigate the potential impacts of future agricultural droughts.

**Author Contributions:** Conceptualization, P.M.; methodology, P.M. and G.A.A.; writing—original draft preparation, P.M. and G.A.A.; writing—review and editing, H.B.M., A.M.K. and G.A.A. All authors have read and agreed to the published version of the manuscript.

**Funding:** This research was funded by the National Research Foundation (NRF) under the grant [MND190403426933].

**Institutional Review Board Statement:** Not applicable.

**Informed Consent Statement:** Not applicable.

**Data Availability Statement:** The data used in this study are available on request.

**Acknowledgments:** Our sincere appreciation goes to the University of Fort Hare, Alice, South Africa for creating an enabling environment for research, and the South African Weather Service (SAWS) and the United States Geological Survey (USGS) for providing data for the study.

**Conflicts of Interest:** No potential conflicts of interest were reported, and all authors have agreed to publish this paper.

## References


1. Correia, C.D.; Amraoui, M.; Santos, J.A. Analysis of the Impacts of Climate Change on Agriculture in Angola: Systematic Literature Review. *Agronomy* **2024**, *14*, 783. [CrossRef]
2. Mpanyaro, Z.; Kalumba, A.M.; Zhou, L.; Afuye, G.A. Mapping and Assessing Riparian Vegetation Response to Drought along the Buffalo River Catchment in the Eastern Cape Province, South Africa. *Climate* **2024**, *12*, 7. [CrossRef]
3. Henchiri, M.; Igbawua, T.; Javed, T.; Bai, Y.; Zhang, S.; Essifi, B.; Ujoh, F.; Zhang, J. Meteorological drought analysis and return periods over north and west Africa and linkage with El Niño–southern oscillation (Enso). *Remote Sens.* **2021**, *13*, 4730. [CrossRef]
4. Afuye, G.A.; Kalumba, A.M.; Busayo, E.T.; Orimoloye, I.R. A bibliometric review of vegetation response to climate change. *Environ. Sci. Pollut. Res.* **2021**, *29*, 1–3. [CrossRef] [PubMed]
5. Tarate, S.B.; Patel, N.R.; Danodia, A.; Pokhariyal, S.; Parida, B.R. Geospatial Technology for Sustainable Agricultural Water Management in India—A Systematic Review. *Geomatics* **2024**, *4*, 91–123. [CrossRef]
6. Li, Q.; Ye, A.; Wada, Y.; Zhang, Y.; Zhou, J. Climate change leads to an expansion of the global drought-sensitive area. *J. Hydrol.* **2024**, *632*, 130874. [CrossRef]
7. Mpala, T.A.; Simatele, M.D. Climate-smart agricultural practices among rural farmers in Masvingo district of Zimbabwe: Perspectives on the mitigation strategies to drought and water scarcity for improved crop production. *Front. Sustain. Food Syst.* **2024**, *7*, 1298908. [CrossRef]
8. Afuye, G.A.; Kalumba, A.M.; Orimoloye, I.R. Characterisation of vegetation response to climate change: A review. *Sustainability* **2021**, *13*, 7265. [CrossRef]
9. Niyonsenga, S.; Eziz, A.; Kurban, A.; Yuan, X.; Umwali, E.D.; Azadi, H.; Hakorimana, E.; Umugwaneza, A.; Fidelis, G.D.; Nsanzabaganwa, J.; et al. Spatiotemporal Analysis of Drought Characteristics and Their Impact on Vegetation and Crop Production in Rwanda. *Remote Sens.* **2024**, *16*, 1455. [CrossRef]
10. FAO. *The State of Food Security and Nutrition in the World: Repurposing Food and Agricultural Policies to Make Healthy Diets More Affordable*; FAO: Rome, Italy, 2022.
11. Javed, T.; Li, Y.; Rashid, S.; Li, F.; Hu, Q.; Feng, H.; Chen, X.; Ahmad, S.; Liu, F.; Pulatov, B. Performance and relationship of four different agricultural drought indices for drought monitoring in China's mainland using remote sensing data. *Sci. Total Environ.* **2021**, *759*, 143530. [CrossRef]
12. Lee, S.J.; Kim, N.; Lee, Y. Development of integrated crop drought index by combining rainfall, land surface temperature, evapotranspiration, soil moisture, and vegetation index for agricultural drought monitoring. *Remote Sens.* **2021**, *13*, 1778. [CrossRef]
13. Quille-Mamani, J.A.; Huayna, G.; Pino-Vargas, E.; Chucuya-Mamani, S.; Vera-Barrios, B.; Ramos-Fernandez, L.; Espinoza-Molina, J.; Cabrera-Olivera, F. Spatio-Temporal Evolution of Olive Tree Water Status Using Land Surface Temperature and Vegetation Indices Derived from Landsat 5 and 8 Satellite Imagery in Southern Peru. *Agriculture* **2024**, *14*, 662. [CrossRef]
14. McKee, T.B.; Doesken, N.J.; Kleist, J. The relationship of drought frequency and duration to time scales. In Proceedings of the 8th Conference on Applied Climatology, Anaheim, CA, USA, 17–22 January 1993; Volume 17, pp. 179–183.
15. Warter, M.M.; Singer, M.B.; Cuthbert, M.O.; Roberts, D.; Caylor, K.K.; Sabathier, R.; Stella, J. Drought onset and propagation into soil moisture and grassland vegetation responses during the 2012–2019 major drought in Southern California. *Hydrol. Earth Syst. Sci.* **2021**, *25*, 3713–3729. [CrossRef]
16. Son, N.T.; Chen, C.F.; Chen, C.R.; Chang, L.Y.; Minh, V.Q. Monitoring agricultural drought in the Lower Mekong Basin using MODIS NDVI and land surface temperature data. *Int. J. Appl. Earth Obs. Geoinf.* **2012**, *18*, 417–427. [CrossRef]
17. Zhou, L.; Wu, J.; Zhang, J.; Zhao, F.; Liu, M.; Zhao, L. Assessing the drought monitoring characteristic of time series NDVI indices in crop growing season. In Proceedings of the 2010 IEEE International Geoscience and Remote Sensing Symposium, Honolulu, HI, USA, 25–30 July 2010; IEEE: Piscataway, NJ, USA; pp. 2063–2066.
18. Manatsa, D.; Mukwada, G.; Siziba, E.; Chinyanganya, T. Analysis of multidimensional aspects of agricultural droughts in Zimbabwe using the Standardized Precipitation Index (SPI). *Theor. Appl. Climatol.* **2010**, *102*, 287–305. [CrossRef]
19. Funk, C.; Budde, M.E. Phenologically-tuned MODIS NDVI-based production anomaly estimates for Zimbabwe. *Remote Sens. Environ.* **2009**, *113*, 115–125. [CrossRef]
20. Falahatkar, S.; Hosseini, S.M.; Soffianian, A.R. The relationship between land cover changes and spatial-temporal dynamics of land surface temperature. *Indian J. Sci. Technol.* **2011**, *4*, 76–81. [CrossRef]
21. Kumar, V.; Sharma, K.V.; Pham, Q.B.; Srivastava, A.K.; Bogireddy, C.; Yadav, S.M. Advancements in drought using remote sensing: Assessing progress, overcoming challenges, and exploring future opportunities. *Theor. Appl. Climatol.* **2024**, *155*, 1–38. [CrossRef]
22. Yousfi, S.; Marín, J.; Parra, L.; Lloret, J.; Mauri, P.V. Remote sensing devices as key methods in advanced turfgrass phenotyping under different water regimes. *Agric. Water Manag.* **2022**, *266*, 107581. [CrossRef]
23. de Lima, I.P.; Jorge, R.G.; de Lima, J.L. Remote sensing monitoring of rice fields: Towards assessing water saving irrigation management practices. *Front. Remote Sens.* **2021**, *2*, 762093. [CrossRef]
24. Nduku, L.; Munghemezulu, C.; Mashaba-Munghemezulu, Z.; Kalumba, A.M.; Chirima, G.J.; Masiza, W.; De Villiers, C. Global research trends for unmanned aerial vehicle remote sensing application in wheat crop monitoring. *Geomatics* **2023**, *3*, 115–136. [CrossRef]

25. Meza, I.; Rezaei, E.E.; Siebert, S.; Ghazaryan, G.; Nouri, H.; Dubovyk, O.; Gerdener, H.; Herbert, C.; Kusche, J.; Popat, E.; et al. Drought risk for agricultural systems in South Africa: Drivers, spatial patterns, and implications for drought risk management. *Sci. Total Environ.* **2021**, *799*, 149505. [CrossRef] [PubMed]
26. Kganvago, M.; Mukhawana, M.B.; Mashalane, M.; Mgabisa, A.; Moloele, S. Recent trends of drought using remotely sensed and in-situ indices: Towards an integrated drought monitoring system for South Africa. In Proceedings of the 2021 IEEE International Geoscience and Remote Sensing Symposium IGARSS, Brussels, Belgium, 11–16 July 2021; IEEE: Piscataway, NJ, USA; pp. 6225–6228.
27. Watson, A.; Miller, J.; Künne, A.; Kralisch, S. Using soil-moisture drought indices to evaluate key indicators of agricultural drought in semi-arid Mediterranean Southern Africa. *Sci. Total Environ.* **2022**, *812*, 152464. [CrossRef] [PubMed]
28. Archer, E.; Landman, W.; Malherbe, J.; Tadross, M.; Pretorius, S. South Africa's winter rainfall region drought: A region in transition? *Clim. Risk Manag.* **2019**, *25*, 100188. [CrossRef]
29. Raphela, T.D.; Pillay, N. Explaining the effect of crop-raiding on food security of subsistence farmers of KwaZulu Natal, South Africa. *Front. Sustain. Food Syst.* **2021**, *5*, 687177. [CrossRef]
30. Bahta, Y.T.; Jordaan, A.; Muyambo, F. Communal farmers' perception of drought in South Africa: Policy implication for drought risk reduction. *Int. J. Disaster Risk Reduct.* **2016**, *20*, 39–50. [CrossRef]
31. Walz, Y.; Min, A.; Dall, K.; Duguru, M.; de Leon, J.C.; Graw, V.; Dubovyk, O.; Sebesvari, Z.; Jordaan, A.; Post, J. Monitoring progress of the Sendai Framework using a geospatial model: The example of people affected by agricultural droughts in Eastern Cape, South Africa. *Prog. Disaster Sci.* **2020**, *5*, 100062. [CrossRef]
32. South African Weather Service. Annual State of the Climate 2022. Pretoria, South Africa. 2023. Available online: https://www.weathersa.co.za/Documents/Corporate/31032023102536.pdf (accessed on 10 July 2023).
33. Ndlazilwana, L.C. Perceptions, Coping Strategies and Welfare Impact of Drought among Small Stock Farmers in Amathole, Eastern Cape. Doctoral Dissertation, North-West University, Potchefstroom, South Africa, 2022.
34. Kloos, S.; Yuan, Y.; Castelli, M.; Menzel, A. Agricultural drought detection with MODIS-based vegetation health indices in southeast Germany. *Remote Sens.* **2021**, *13*, 3907. [CrossRef]
35. Shinga, P.S.; Tesfamichael, S.G.; Sibandze, P.; Kalumba, A.M.; Afuye, G.A. Modelling spatiotemporal patterns of wildfire risk in the Garden Route District biodiversity hotspots using analytic hierarchy process in South Africa. *Nat. Hazards* **2024**, 1–25. [CrossRef]
36. Jaber, S.M. Insights About the Spatial and Temporal Characteristics of the Relationships Between Land Surface Temperature and Vegetation Abundance and Topographic Elements in Arid to Semiarid Environments. *Remote Sens. Earth Syst. Sci.* **2023**, *6*, 254–274. [CrossRef]
37. Amahlathi Local Municipality Integrated Development Plan. Available online: https://www.amahlathi.gov.za/wp-content/uploads/2023/06/Final-IDP-2023-2024.pdf (accessed on 5 July 2023).
38. Bicheron, P.; Amberg, V.; Bourg, L.; Petit, D.; Huc, M.; Miras, B.; Brockmann, C.; Hagolle, O.; Delwart, S.; Ranera, F.; et al. Geolocation assessment of MERIS GlobCover orthorectified products. *IEEE Trans. Geosci. Remote Sens.* **2011**, *49*, 2972–2982. [CrossRef]
39. Afuye, G.A.; Kalumba, A.M.; Owolabi, S.T.; Thamaga, K.H.; Ndou, N.; Sibandze, P.; Orimoloye, I.R. Analyzing spatiotemporal variations and dynamics of vegetation over Amathole district municipality in South Africa. *Environ. Dev. Sustain.* **2024**, 1–26. [CrossRef]
40. Klisch, A.; Atzberger, C. Operational drought monitoring in Kenya using MODIS NDVI time series. *Remote Sens.* **2016**, *8*, 267. [CrossRef]
41. Mogonong, B.P.; Twine, W.; Feig, G.T.; Van der Merwe, H.; Fisher, J.T. Influences of Climate Variability on Land Use and Land Cover Change in Rural South Africa. *Remote Sens.* **2024**, *16*, 1200. [CrossRef]
42. Tadesse, A.; Tolossa, D.; Tsehaye, S.; Yayeh, D. Dynamics of Land Use and Land Cover Changes in Amibara and Awash-Fentale Districts, Ethiopia. *Remote Sens. Appl. Soc. Environ.* **2024**, *36*, 101315. [CrossRef]
43. Sun, X.; Zhou, Y.; Jia, S.; Shao, H.; Liu, M.; Tao, S.; Dai, X. Impacts of mining on vegetation phenology and sensitivity assessment of spectral vegetation indices to mining activities in arid/semi-arid areas. *J. Environ. Manag.* **2024**, *356*, 120678. [CrossRef]
44. Dyosi, M.; Kalumba, A.M.; Magagula, H.B.; Zhou, L.; Orimoloye, I.R. Drought conditions appraisal using geoinformatics and multi-influencing factors. *Environ. Monit. Assess.* **2021**, *193*, 365. [CrossRef]
45. Lottering, S.; Mafongoya, P.; Lottering, R. Detecting and mapping drought severity using multi-temporal Landsat data in the uMsinga region of KwaZulu-Natal, South Africa. *Geocarto Int.* **2022**, *37*, 1574–1586. [CrossRef]
46. Marumbwa, F.M.; Cho, M.A.; Chirwa, P.W. Geospatial analysis of meteorological drought impact on Southern Africa biomes. *Int. J. Remote Sens.* **2021**, *42*, 2155–2173. [CrossRef]
47. United States Geological Survey. Landsat 8 (L8) Data Users' Handbook Version 5.0. USGS, 2019. Available online: https://d9-wret.s3.us-west-2.amazonaws.com/assets/palladium/production/s3fs-public/atoms/files/LSDS-1574_L8_Data_Users_Handbook-v5.0.pdf (accessed on 12 July 2023).
48. Yıldırım, T.; Asık, S. Index-based assessment of agricultural drought using remote sensing in the semi-arid region of Western Turkey. *J. Agric. Sci.* **2018**, *24*, 510–516.
49. Kakembo, V.; Ndou, N. Relating vegetation condition to grazing management systems in the central Keiskamma Catchment, Eastern Cape Province, South Africa. *Land Degrad. Dev.* **2019**, *30*, 1052–1060. [CrossRef]

50. Botai, C.M.; Botai, J.O.; Adeola, A.M.; De Wit, J.P.; Ncongwane, K.P.; Zwane, N.N. Drought risk analysis in the Eastern Cape Province of South Africa: The copula lens. *Water* **2020**, *12*, 1938. [CrossRef]
51. Mukhawana, M.B.; Kanyerere, T.; Kahler, D. Review of in-situ and remote sensing-based indices and their Applicability for integrated drought monitoring in South Africa. *Water* **2023**, *15*, 240. [CrossRef]
52. Nkamisa, M.; Ndhleve, S.; Nakin, M.D.; Mngeni, A.; Kabiti, H.M. Analysis of trends, recurrences, severity and frequency of droughts using standardised precipitation index: Case of OR Tambo District Municipality, Eastern Cape, South Africa. *Jàmbá-J. Disaster Risk Stud.* **2022**, *14*, 1147. [CrossRef]
53. Tran, T.V.; Bruce, D.; Huang, C.Y.; Tran, D.X.; Myint, S.W.; Nguyen, D.B. Decadal assessment of agricultural drought in the context of land use land cover change using MODIS multivariate spectral index time-series data. *GIScience Remote Sens.* **2023**, *60*, 2163070. [CrossRef]
54. Zhao, Y.; Zhang, J.; Bai, Y.; Zhang, S.; Yang, S.; Henchiri, M.; Seka, A.M.; Nanzad, L. Drought monitoring and performance evaluation based on machine learning fusion of multi-source remote sensing drought factors. *Remote Sens.* **2022**, *14*, 6398. [CrossRef]
55. Kumari, K.; Yadav, S. Linear regression analysis study. *J. Pract. Cardiovasc. Sci.* **2018**, *4*, 33–36. [CrossRef]
56. Pavlidis, V.; Kganyago, M.; Mukhawana, M.; Alexandridis, T.; Cherif, I.; Laneve, G.; Orsi, R.; Kartsios, S.; Karypidou, M.C.; Sofiadis, I.; et al. A drought monitoring and early warning service for food security in South Africa. *Clim. Serv.* **2024**, *34*, 100463. [CrossRef]
57. Bhaga, T.D.; Dube, T.; Shekede, M.D.; Shoko, C. Impacts of climate variability and drought on surface water resources in Sub-Saharan Africa using remote sensing: A review. *Remote Sens.* **2020**, *12*, 4184. [CrossRef]
58. Orimoloye, I.R.; Afuye, G.; Obateru, R.; Bodunrin, I.R.; Babalola, T.; Olusola, A.O. Drought in a semi-arid Environment: A Decadal Drought Assessment Using Earth Observation Information. *Front. Environ. Sci.* **2024**, *12*, 1414336.
59. Ekundayo, O.Y.; Okogbue, E.C.; Akinluyi, F.O.; Kalumba, A.M.; Orimoloye, I.R. Geoinformatics approach to desertification evaluation using vegetation cover changes in the Sudan-Sahelian region of Nigeria from 2000 to 2010. In *Re-Envisioning Remote Sensing Applications*; CRC Press: Boca Raton, FL, USA, 2021; pp. 261–270.
60. Afuye, G.A.; Kalumba, A.M.; Ishola, K.A.; Orimoloye, I.R. Long-term dynamics and response to climate change of different vegetation types using GIMMS NDVI3g data over Amathole district in South Africa. *Atmosphere* **2022**, *13*, 620. [CrossRef]
61. Willie, Y.A.; Pillay, R.; Zhou, L.; Orimoloye, I.R. Monitoring spatial pattern of land surface thermal characteristics and urban growth: A case study of King Williams using remote sensing and GIS. *Earth Sci. Inform.* **2019**, *12*, 447–464. [CrossRef]
62. Orimoloye, I.R.; Ololade, O.O.; Belle, J.A. Spatio-Environmental Distribution of Drought Disaster Events: A Space-Based Approach Using Terra-MODIS Vegetation Index. In *Re-Envisioning Advances in Remote Sensing*; CRC Press: Boca Raton, FL, USA, 2022; pp. 105–119.
63. Thamaga, K.H.; Gom, S.; Adesola, G.O.; Ndou, N.; Muavhi, N.; Mndela, M.; Sibandze, P.; Abdo, H.G.; Maphanga, T.; Afuye, G.; et al. Integration of Geospatial-Based Algorithms for Groundwater Potential Characterization in Keiskamma Catchment of South Africa. *Groundw. Sustain. Dev.* **2024**, *26*, 101262. [CrossRef]
64. Orimoloye, I.R.; Ololade, O.O.; Mazinyo, S.P.; Kalumba, A.M.; Ekundayo, O.Y.; Busayo, E.T.; Akinsanola, A.A.; Nel, W. Spatial assessment of drought severity in Cape Town area, South Africa. *Heliyon* **2019**, 5. [CrossRef] [PubMed]
65. Afuye, G.A.; Nduku, L.; Kalumba, A.M.; Santos, C.A.; Orimoloye, I.R.; Ojeh, V.N.; Thamaga, K.H.; Sibandze, P. Global trend assessment of land use and land cover changes: A systematic approach to future research development and planning. *J. King Saud Univ. Sci.* **2024**, *36*, 103262. [CrossRef]
66. Gaznayee, H.A.; Al-Quraishi, A.M.; Mahdi, K.; Ritsema, C. A geospatial approach for analysis of drought impacts on vegetation cover and land surface temperature in the Kurdistan Region of Iraq. *Water* **2022**, *14*, 927. [CrossRef]
67. Rafiei Sardooi, E.; Azareh, A.; Eskandari Damaneh, H.; Skandari Damaneh, H. Drought Monitoring Using MODIS Land Surface Temperature and Normalized Difference Vegetation Index Products in Semi-Arid Areas of Iran. *J. Rangel. Sci.* **2021**, *11*, 402–418.
68. Hazaymeh, K.; Hassan, Q.K. Remote sensing of agricultural drought monitoring: A state-of-the-art review. *AIMS Environ. Sci.* **2016**, *3*, 604–630. [CrossRef]
69. Mutengwa, C.S.; Mnkeni, P.; Kondwakwenda, A. Climate-smart agriculture and food security in Southern Africa: A review of the vulnerability of smallholder agriculture and food security to climate change. *Sustainability* **2023**, *15*, 2882. [CrossRef]
70. Ha, T.V.; Uereyen, S.; Kuenzer, C. Agricultural drought conditions over mainland Southeast Asia: Spatiotemporal characteristics revealed from MODIS-based vegetation time-series. *Int. J. Appl. Earth Obs. Geoinf.* **2023**, *121*, 103378. [CrossRef]
71. Sofia, G.; Zaccone, C.; Tarolli, P. Agricultural drought severity in NE Italy: Variability, bias, and future scenarios. *Int. Soil Water Conserv. Res.* **2024**, *12*, 403–418. [CrossRef]
72. Botai, C.M.; Botai, J.O.; Adeola, A.M. Spatial distribution of temporal precipitation contrasts in South Africa. *South Afr. J. Sci.* **2018**, *114*, 70–78. [CrossRef] [PubMed]